Supporting Information

Scharte et al. 10.1073/pnas.0812902106

SI Methods

Cloning of cP2-Expression Constructs. To obtain cDNA fragments without transit sequence of *Arabidopsis* P2-type *G6PD* isoform (At1g24280), total RNA was isolated from *Arabidopsis* (Col) (grown on 2% sucrose-containing MS medium, pH 5.6, 16-h photoperiod with 24 °C day/18 °C night regime). Reverse transcription used a poly(A) primer mix (5′-A_{30}C/G/T-3′) and SuperScript II (Invitrogen), according to the protocol. Truncated cDNA fragments (lacking 5′ 195 bp) were amplified with PfuI DNA polymerase (Stratagene) and ZM_S2 (5′-N_6GGATCCAAG**ATG**GTTGTCGTGCAAGATGGATCAGTAGCCACC-3′) plus ZM_A3 (5′-N_6GTCGAC**TCA**CTGATCAAGACTTAGGTCTCCCCATTG-3′) primers, and directly cloned into BamHI- and SalI-opened pBluescript SK vector (Stratagene), yielding pZM3. Similarly, cP2 fragments were introduced into the multiple cloning site of pA35 (1) between cauliflower mosaic virus 35S promoter and OCS polyadenylation signal, yielding pZM4. The entire expression cassette was transferred by HindIII and partial PvuII digestion into HindIII/SnaBI-opened binary vector pGSC1704 [HygR] (Plant Genetic Systems), yielding final construct pZM5 suited for stable *Agrobacterium*-mediated plant transformation.

For *Escherichia coli* expression vector pET16b (Novagen), cP2 cDNA fragments were amplified from pZM4 with Phusion DNA polymerase (Finzymes) and primers pET-cP2 sense (without His tag, NcoI underlined: 5′-NNNCC**ATG**GTTGTCGTGCAAGATGGATCAGTAG-3′) and ZM_A3 antisense (see above). NcoI/SalI-digested PCR products were first cloned in *E. coli* XL1 Blue (Stratagene) after ligation to NcoI/XhoI-opened pET16b (Novagen), yielding pET-cP2. G6PDH activity of the cP2 enzyme was determined in a G6PDH-deficient *E. coli* strain (2). Expression of cP2 was induced (1 mM IPTG) in logarithmically growing cultures, harvested by centrifugation after 2–3 h of growth at 37 °C, and adjusted to OD_{600} of 10. Pelleted cells were extracted in 100 mM NaH_2PO_4, 10 mM Tris-NaOH (pH 8), 0.1 mM Pefabloc SC, and 0.02 mM NADP (to stabilize G6PDH activity) by sonication 3 times for 10 s at 50 W (Branson).

Cloning of a Xanthi-Specific cyt*G6PD*-RNAi Construct. The RNAi construct was designed based on tobacco cytosolic *G6PD* isoforms (3). Approximately 400 bp of target sequence was amplified by RT-PCR from total RNA (described above) isolated from Xanthi source leaves with Phusion DNA polymerase using primers cyt*G6PD*-sense (SalI underlined: 5′-CACCGTCGACAATATGAAGGCTATAAGGATGACC-3′) and cyt*G6PD*-antisense (BamHI underlined: 5′-GGATCCTATATGACAGGTCTAATTCACTTTGAAC-3′). PCR fragments were inserted twice into vector pUC-RNAi. Then, the entire dsRNAi region was released by PstI and inserted into SdaI opened binary vector pBinAR[Kan] (4).

1. Wenderoth I, von Schaewen A (2000) Isolation and characterization of plant N-acetyl glucosaminyltransferase I (*Gnt*) cDNA sequences. Functional analyses in the Arabidopsis *cgl* mutant and in antisense plants. *Plant Physiol* 123:1097–1108.
2. Wenderoth I, Scheibe R, von Schaewen A (1997) Identification of the cysteine residues involved in redox modification of plant plastidic glucose-6-phosphate dehydrogenase. *J Biol Chem* 272:26985–26990.
3. Wendt UK, Hauschild R, Lange C, Pietersma M, Wenderoth I, von Schaewen A (1999) Evidence for functional convergence of redox regulation in G6PDH isoforms of cyanobacteria and higher plants. *Plant Mol Biol* 40:487–494.
4. Chen S, Hofius D, Sonnewald U, Börnke F (2003) Temporal and spatial control of gene silencing in transgenic plants by inducible expression of double-stranded RNA. *Plant J* 36:731–740.
5. Wendt UK, Wenderoth I, Tegeler A, von Schaewen A (2000) Molecular characterization of a novel glucose-6-phosphate dehydrogenase from potato (*Solanum tuberosum* L.). *Plant J* 23:723–733.
6. von Schaewen A, Langenkamper G, Graeve K, Wenderoth I, Scheibe R (1995) Molecular characterization of the plastidic glucose-6-phosphate dehydrogenase from potato in comparison to its cytosolic counterpart. *Plant Physiol* 109:1327–1335.
7. Scharte J, Schön H, Weis E (2005) Photosynthesis and carbohydrate metabolism in tobacco leaves during an incompatible interaction with *Phytophthora nicotianae*. *Plant Cell Environ* 28:1421–1435.
8. Meng Q, et al. (2001) Sink-source transition in tobacco leaves visualized using chlorophyll fluorescence imaging. *New Phytol* 151:585–595.
9. Schnarrenberger C, Flechner A, Martin W (1995) Enzymatic evidence for a complete oxidative pentose phosphate pathway in chloroplasts and an incomplete pathway in the cytosol of spinach leaves. *Plant Physiol* 108:609–614.
10. Eicks M, Maurino V, Knappe S, Flügge UI, Fischer K (2002) The plastidic pentose phosphate translocator represents a link between the cytosolic and the plastidic pentose phosphate pathways in plants. *Plant Physiol* 128:512–522.
11. Tetlow IJ, Blissett KJ, Emes MJ (1998) Metabolite pools during starch synthesis and carbohydrate oxidation in amyloplasts isolated from wheat endosperm. *Planta* 204:100–108.

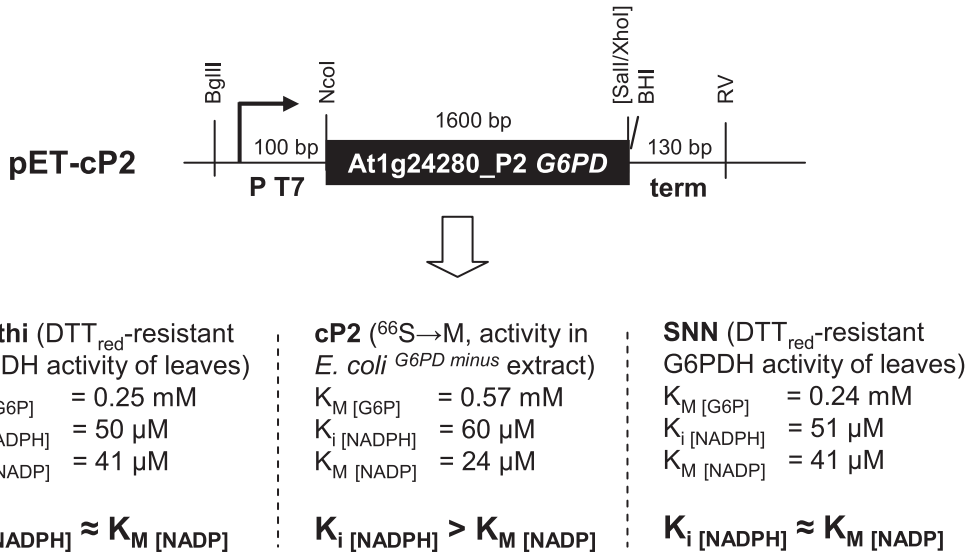

Fig. S1. Biochemical characteristics of cP2 versus tobacco cytosolic G6PDH. Kinetic parameters were determined for the recombinant cP2 enzyme after extraction from an *E. coli* G6PDH-minus strain (2) and compared with the DTT_{red}-resistant (cytosolic) G6PDH activity extracted from source leaves of WT tobacco Xanthi and SNN cultivars ($n \geq 3$). Leaf discs were frozen and crushed in liquid nitrogen and extracted in 100 mM Tris maleate buffer (pH 8), which inhibits 6PGDH, with 280 mM 2-mercaptoethanol. Extracts were centrifuged twice at high speed (4 °C) and supernatants were adjusted to 62.5 mM DTT_{red} (in 100 mM Tris maleate, pH 8) followed by 30-min preincubation at room temperature (to inhibit plastidic isoenzymes), before measuring G6PDH activity by A_{340} in a double-wavelength spectrophotometer (Beckman DU 650, automatic subtraction of A_{405}). Standard tests contained 0.2 mM NADP in 100 mM Tris maleate (pH 8). Minor rates recorded over 5 min before starting reactions with glucose 6-phosphate (G6P) were subtracted. Kinetic parameters were determined as described previously (5). K_i values for NADPH (at 0, 50, 70, or 100 μM) were assayed in the presence of NADP (at 0, 30, 60, 90, 120, or 150 μM) at saturating G6P (2 mM).

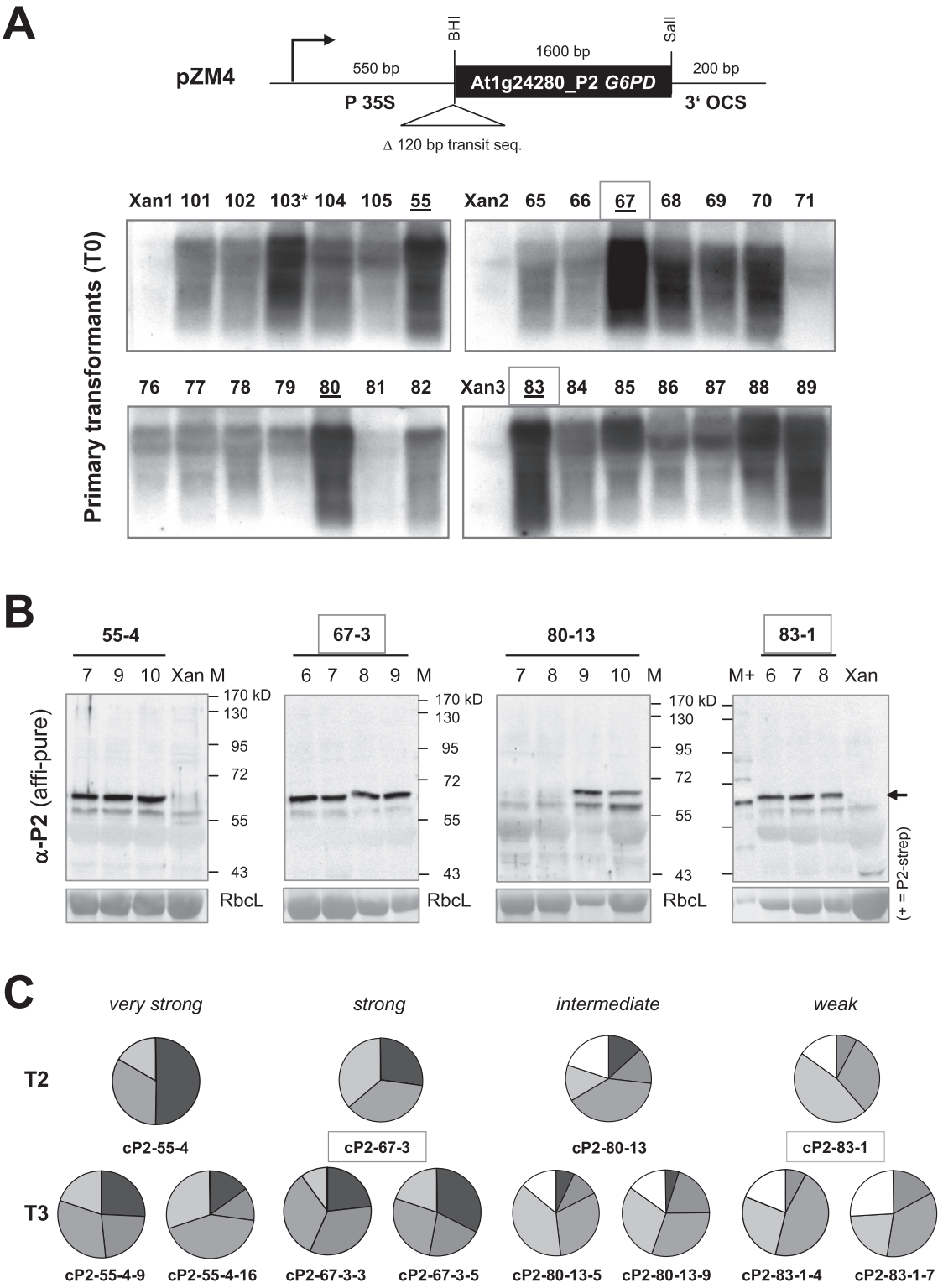

Fig. S2. Expression and immunoblot analysis of the Xanthi::cP2 lines plus stability of lesion formation. (*A*) Expression cassette of the binary vector construct used for the generation of Xanthi::cP2 lines, and Northern blot analysis of primary transformants (T_0) using ^{32}P-labeled P2-cDNA fragments as described in ref. 6. (*B*) Immunoblot analyses of the T_2 progeny of very strong (55-4), strong (67-3), intermediate (80-13), and weak (83-1) cP2 lines. (*C*) Stability of lesion formation in the corresponding T_3 progeny. The cP2 lines marked by a frame were chosen for the RNAi approach.

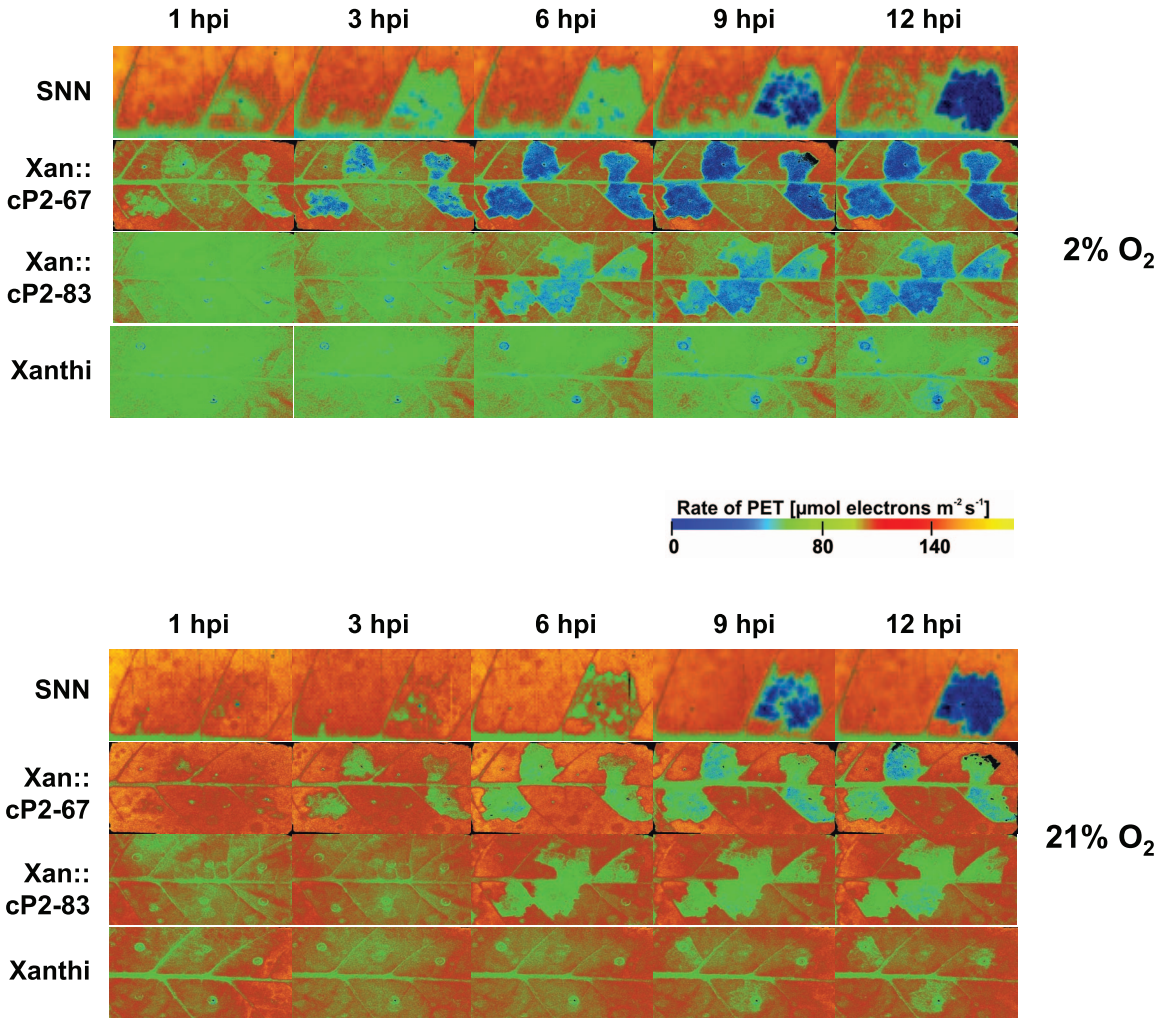

Fig. S3. Defense-induced inhibition of photosynthesis in the Xanthi::cP2 lines. The formation of hypersensitive lesions was preceded by defense-induced inhibition of photosynthesis, as visualized by chlorophyll-*a* fluorescence imaging (7). Transgenic Xanthi::cP2 lines behave more like the resistant cultivar SNN, whereas in susceptible Xanthi WT leaves no depression of photosynthesis is detected. Decline in photosynthesis is an integral part of the metabolic transitions that accompany plant defense and hypersensitive cell death, and it involves 2 steps. Early during infection, stomata at the infection sites close (compare Fig. 2*C*) and the rate of CO_2-dependent photosynthetic electron transport (PET) decreases. This was analyzed by measuring PET in the presence of low oxygen (2% O_2), enhanced CO_2 concentration (700 μL of CO_2 per L), and nearly saturating light (820 μmol of quanta m^{-2} s^{-1}). Under such conditions, photorespiration is largely suppressed (whereas mitochondrial respiration is not), and electrons are mostly consumed by CO_2 fixation (7). In the presence of ambient oxygen (21% O_2), when electrons are consumed either by CO_2 fixation or by photorespiration, only weak inhibition was recorded during the first 6 hpi, but later photosynthetic flux equally decreased in the presence or absence of high oxygen. The O_2-insensitive decline observed at later time points (>6 hpi) reflects a general decline of photosynthetic capacity in infected tissue, probably due to depression of the high-potential chain (7) or the Calvin cycle.

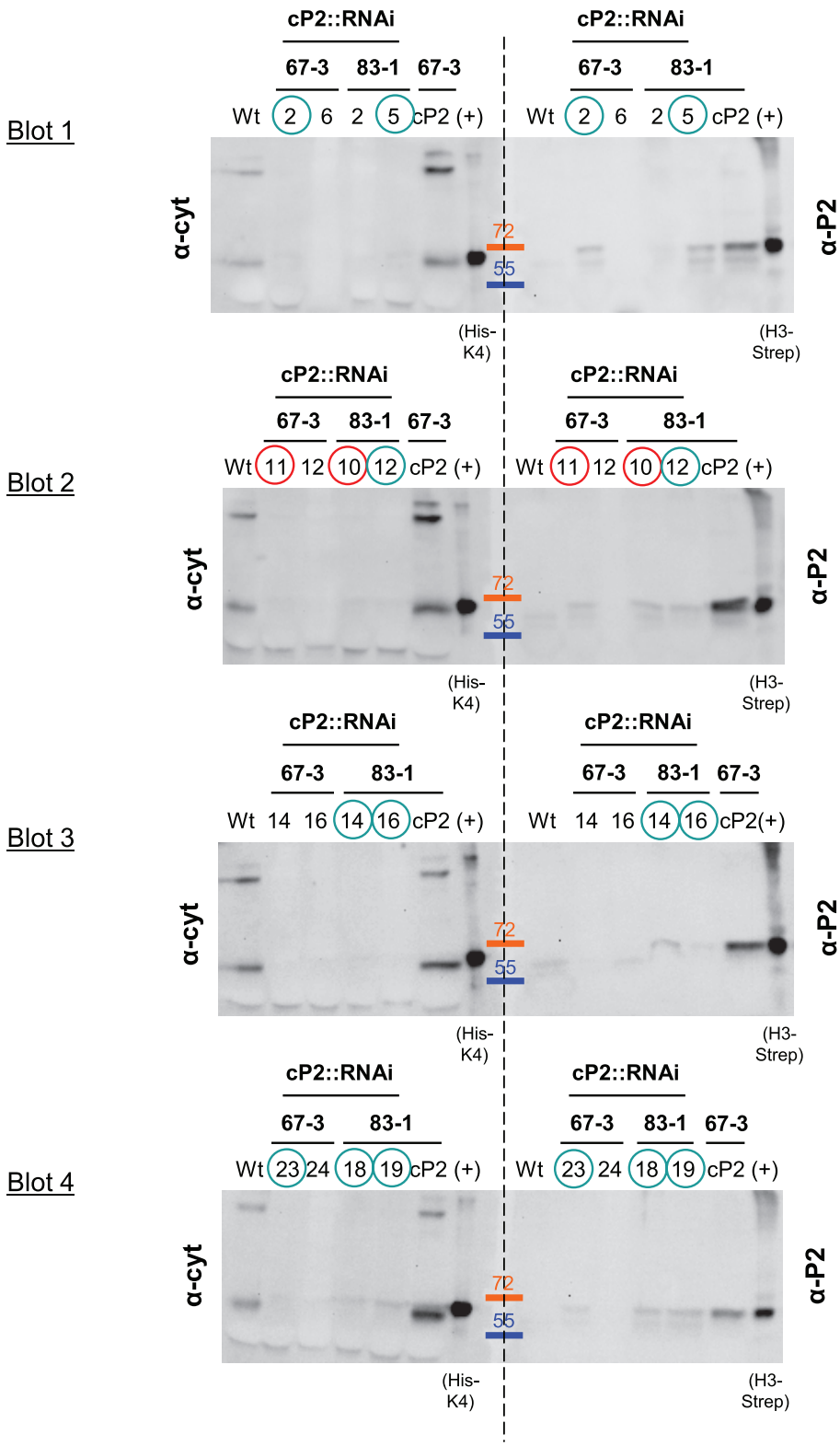

Fig. S4. Selection of isoenzyme-replaced Xanthi transformants. Immunoblot analyses of primary Xanthi::cP2::RNAi transformants (T_0) with G6PDH isoform-specific antisera (6). Blots were cut along the dashed line before development. Positions of 2 molecular mass standards are shown (72 and 55 kDa). Supertransformed plants that lacked cytosolic G6PDH but retained cP2 signals were selected, and those circled were used for further analyses.

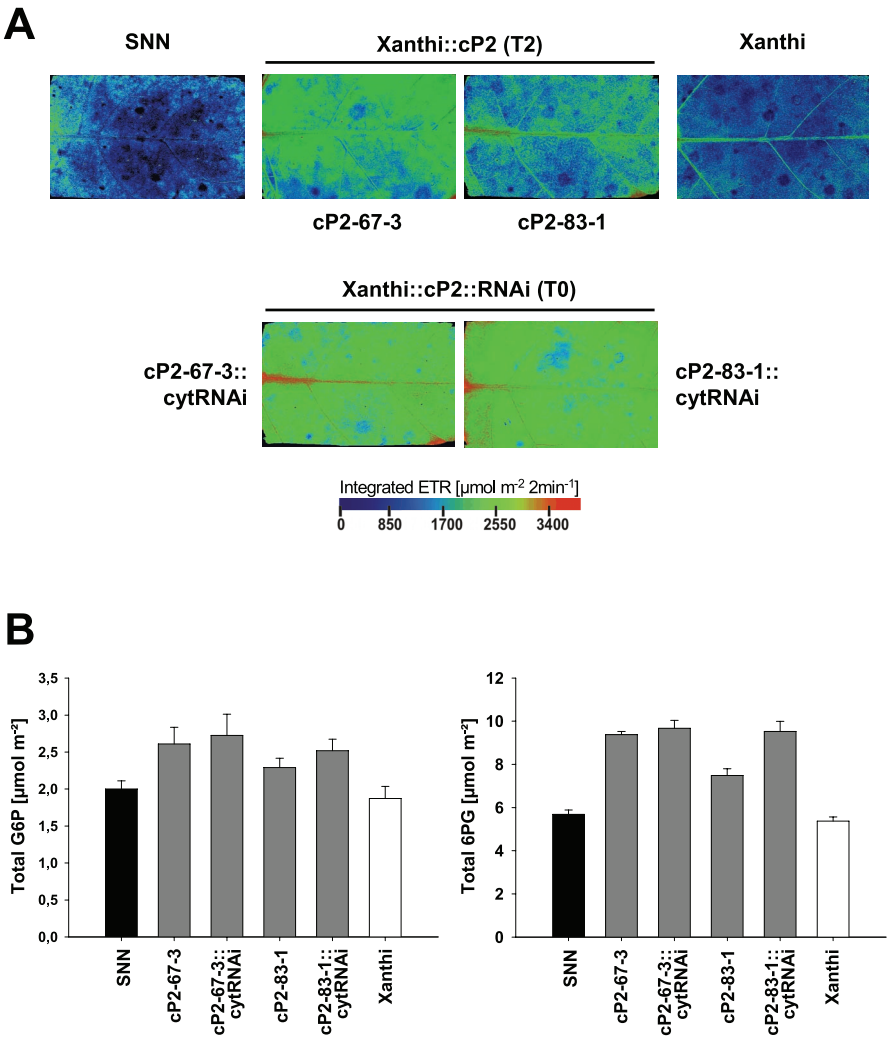

Fig. S5. Metabolic analyses of cP2 overexpressors and isoenzyme-replaced Xanthi lines. (*A*) Photosynthetic induction in water-infiltrated (control) sources leaves of SNN and Xanthi WT plants, cP2 overexpressors, and isoenzyme-replaced Xanthi lines after a 16-h dark period. The representative images are derived from chlorophyll-*a* fluorescence, as described (8). ETR, electron transport rate. Photosynthetic induction was shown previously to be a robust indicator of oxidative pentose-phosphate pathway (OPPP) metabolite pools at the end of a dark period, preceding illumination (8). The OPPP shares metabolites with the ribulose 1,5-bisphosphate regenerative part of the Calvin cycle. Because normally OPPP activity in source leaves is low, onset of the Calvin cycle is limited by availability of shared metabolites. Therefore, induction of photosynthesis is slow, in particular at low CO_2. Activation of the OPPP in the dark, however, leads to an increase in metabolite levels required for rapid induction of photosynthesis. In plants, OPPP reactions occur partly in the cytosol (oxidative branch) and completely in the chloroplast stroma (9). These metabolite pools communicate via sugar-phosphate carriers in the chloroplast envelope, leading to equilibration between cytosol and plastid stroma, where they are shared with the Calvin cycle (10). Thus, elevated flux through the oxidative OPPP reactions (resulting from increased G6PDH activity in the cytosol) raises stromal Calvin cycle intermediates, which facilitate the induction of photosynthesis. Fast photosynthetic induction has actually been observed in developing tobacco tissue at the base of expanding leaves, which constitute carbohydrate-consuming sink zones that display high dark levels of stromal sugar-phosphate intermediates, such as 3PGA (8). Photosynthetic induction was routinely analyzed during the first 2 min after a dark period (>1 h). Measurements of photosynthetic induction were performed in 21% O_2 and 65 μL of CO_2 per L (close to the CO_2-compensation point). Under such conditions, stomatal aperture was shown to have no effect on photosynthetic induction (8). Thus, chlorophyll-*a* fluorescence imaging visualizes photosynthetic induction in situ and at real time: low values (blue) indicate slow induction; high values (green to red) indicate fast induction. Interestingly, accelerated photosynthetic induction not only was recorded after infection (see Figs. 2*E* and 3*D*) but also was found to be generally elevated in leaves of the Xanthi::cP2 transformants (green background). Even stronger induction in the isoenzyme-replaced Xanthi lines is in accordance with permanently elevated OPPP metabolite levels in the transformants, equilibrating between cytosol and chloroplast stroma. (*B*) Determination of G6PDH substrate and product levels. Measurement of 6-phosphogluconate (6PG) and glucose 6-phosphate (G6P) contents were performed in a sequential assay according to Tetlow et al. (11). Both metabolites ([G6P + 6PG]) increased in the transgenic Xanthi lines compared with those in WT plants, but the increase was most pronounced in the isoenzyme-replaced lines (≈50% increase). Parallel to the elevated metabolite levels, the 6PG/G6P ratio increased from 2.8 (WT) to ≈3.8 in the isoenzyme-replaced Xanthi lines. Note that there were no significant differences in both 6PG/G6P and absolute metabolite levels between SNN and Xanthi WT cultivars. Increase in 6PG/G6P (product/substrate) reflects elevated G6PDH activity (and related NADPH generation) in the cytosol. As a consequence of elevated cytosolic G6PDH activity, the total level of both cytosolic and stromal OPPP metabolites will increase, because metabolites downstream of the oxidative OPPP branch equilibrate with those in the chloroplast stroma (via C5 sugar-P transporter XPT) and replenish stromal OPPP pools. Elevated levels of OPPP metabolites are also reflected by photosynthetic induction (see *A*). It should be noted that metabolite levels in the different transgenic lines mirror not only the level of pathogen response but also the extent of drought tolerance (Fig. 3) and floral development (Fig. S7).

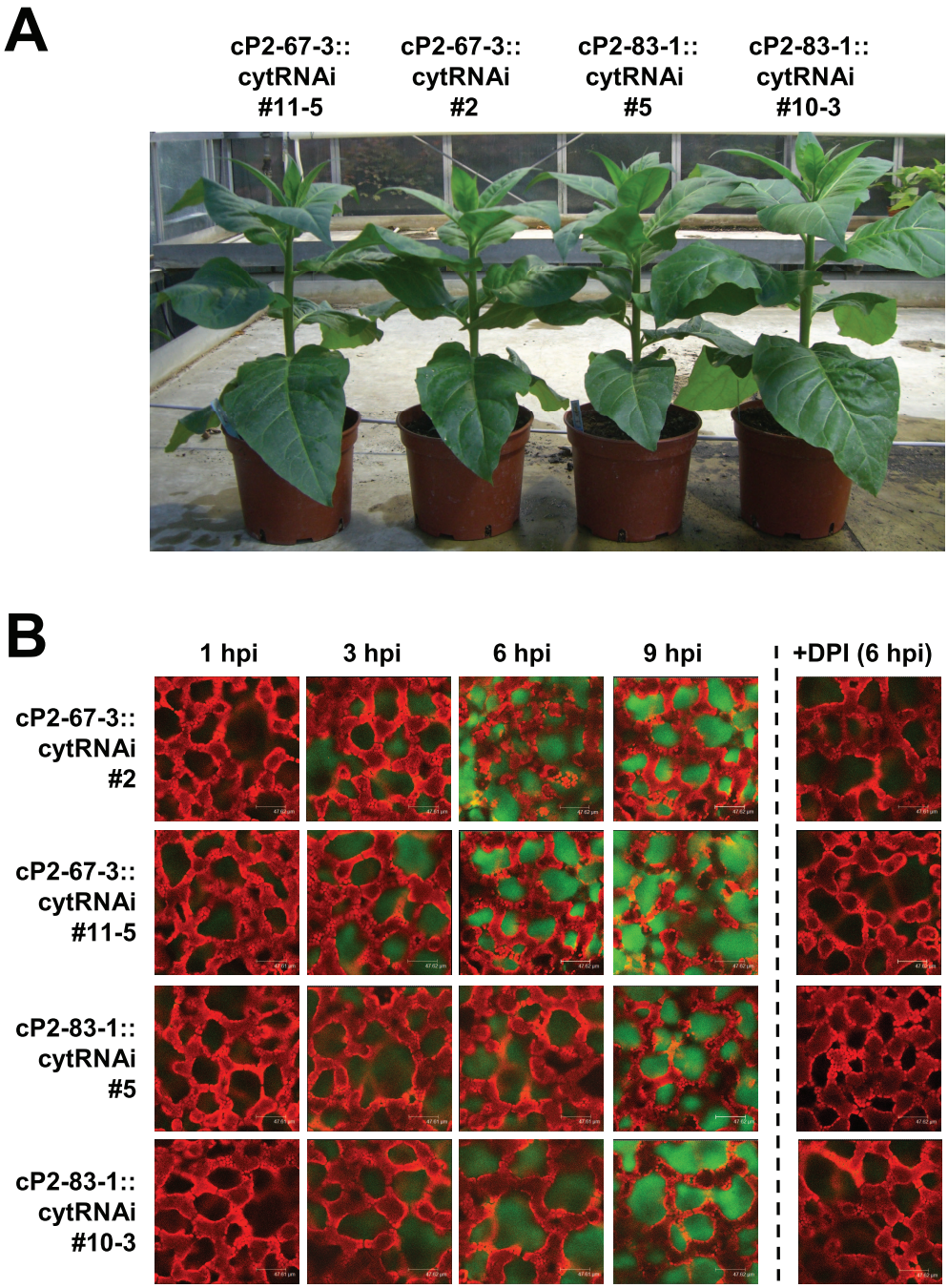

Fig. S6. ROS analyses of selected isoenzyme-replaced Xanthi lines. Side-by-side photo of 5-week-old RNAi supertransformants (T_0 versus T_1) in the greenhouse, before their transfer to climate-controlled growth chambers for later measurement of pathogen-induced ROS release. Growth habit (*A*) as well as defense-induced ROS release (*B*) was much more homogenous in the isoenzyme-replaced Xanthi lines compared with the parental cP2 lines (T_2 progeny of cP2-67-3 and cP2-83-1). For further explanation, see legend to Fig. 2.

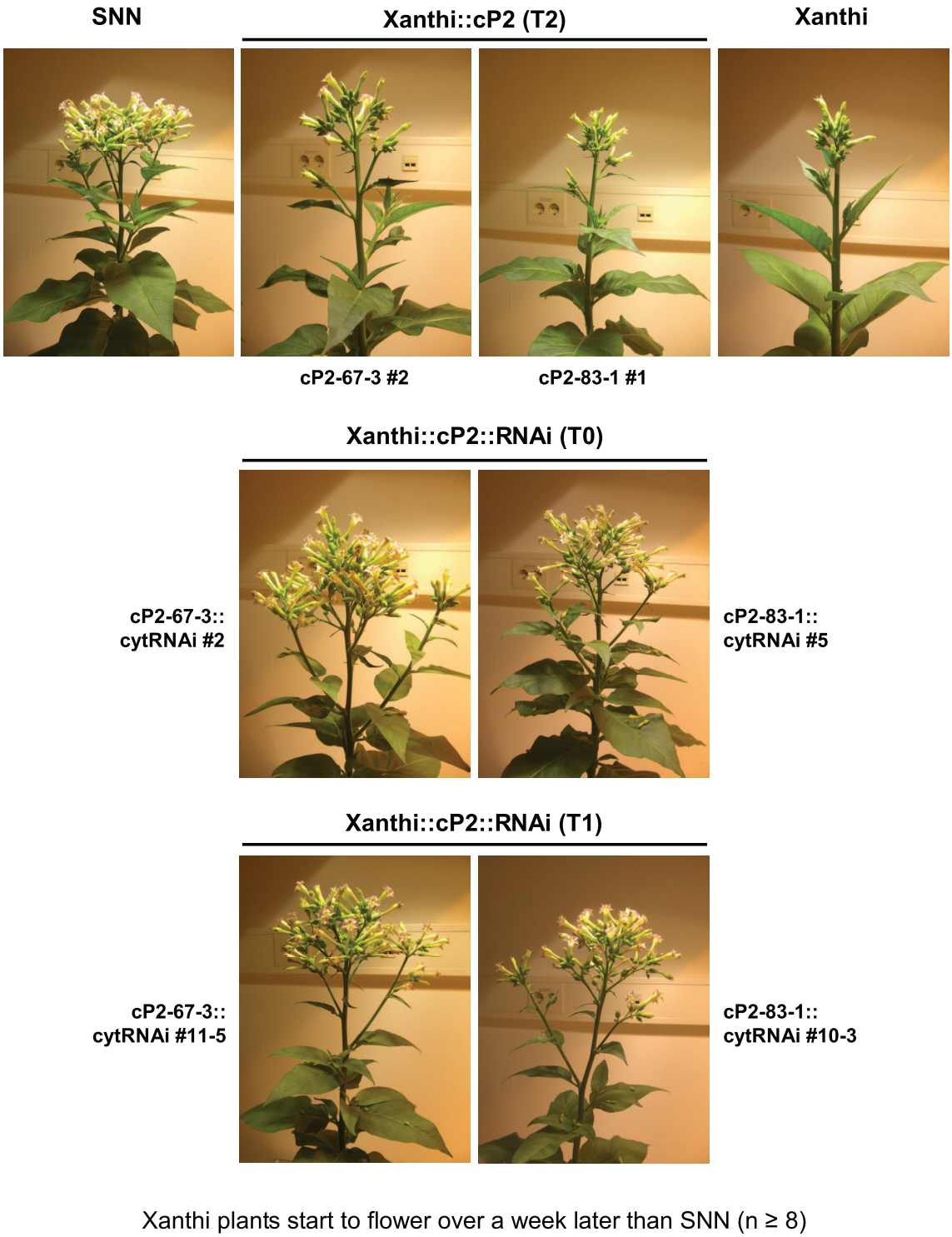

Fig. S7. Flower development in cP2 overexpressors versus isoenzyme-replaced lines. Onset of flowering reflects the general tendency of the isoenzyme-replaced Xanthi lines to respond like the resistant tobacco cultivar SNN. Inflorescences of the parental cP2 lines are shown between SNN and Xanthi WT, with T_0 and T_1 individuals of the isoenzyme-replaced (cP2::RNAi) Xanthi lines underneath.